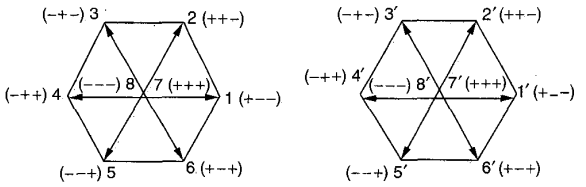

Fig. 2 *Space phasor locations for inverter-1 (left) and inverter-2 (right)*

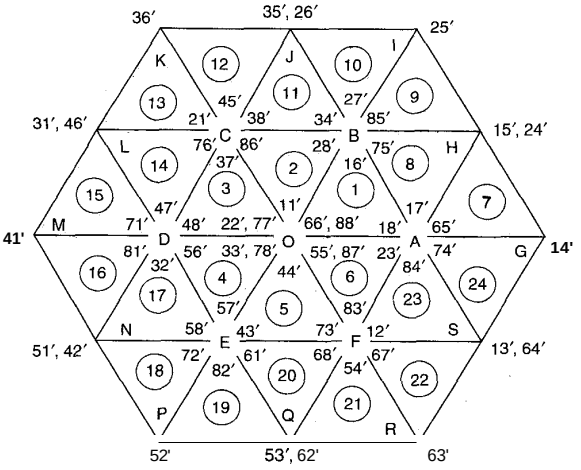

Fig. 3 *Voltage space phasor combinations from dual-inverter scheme*

In Fig. 3 |OA| represents the DC link voltage of individual inverters, and is equal to $V_{DC}/2$, while |OG| represents the DC link voltage of an equivalent single inverter drive, and is equal to V_{DC}. A total of 64 space phasor combinations are possible from the dual inverter configuration, as each inverter is capable of assuming eight states independently of the other. For the primitive scheme shown in Fig. 1, a significant triplen harmonic content in the inverter phase currents is expected because of the lack of an isolated neutral point.

The triplen harmonic content in the phase voltage in the dual inverter scheme shown in Fig. 1 depends on the space phasor combinations used [5, 6]. The triplen harmonic content in the phase voltage in this scheme from different space phasor combinations is shown in Table 1.

There are 20 space phasor combinations with a third harmonic contribution of zero (Table 1). If these space phasor combinations are used exclusively, the magnitude of the fundamental component is reduced (Fig. 3). However, by giving an additional boost to the DC link voltage it is possible to obtain the rated phase voltage of the motor from the dual inverter configuration. The required value for the DC link voltage may be obtained by determining the maximum phase voltage that can be obtained from the voltage space phasor with a length equal to the radius of the circle inscribed in hexagon HJLNQS (Fig. 3).

3 Dual inverter with auxiliary switches

The proposed power circuit schematic is shown in Fig. 4. Auxiliary switches SW_1 to SW_4 are bidirectional, inserted to block the triplen harmonic currents by creating a switched neutral for certain space phasor Combinations. From Table 1, it may be observed that there are certain space phasor combinations that would not contribute to the zero sequence voltages (ex: 1–5′, 2–4′, etc.). For these combinations, SW_1 to SW_4 may be closed without zero sequence currents resulting. Other combinations that may be used are the ones with a zero state at one end of the load phase (ex: 7–4′, 5–8′, etc.). When one of the inverters is clamped to a zero state (+++ or −−−), auxiliary switches connecting that inverter to the DC bus are opened, creating an isolated switched neutral. Under these conditions the zero sequence currents cannot flow for lack of a return path, but for positive and the negative sequence currents (where $i_a + i_b + i_c = 0$), the return path is provided by the zero-state switched inverter. It may be observed that the rest of the space phasor combinations cannot be used in this strategy (ex: 1–4′, 2–3′, and 5–5′, etc.), as these combinations do not contain a zero state for any of the inverters and hence

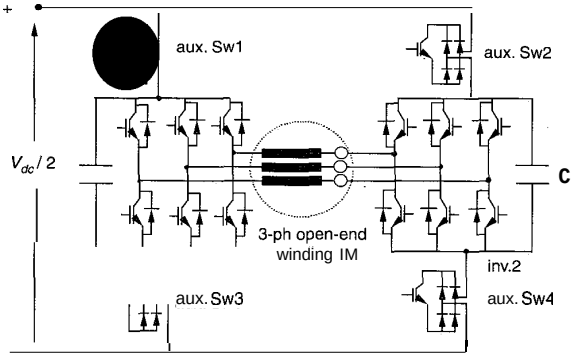

Fig. 4 *Proposed power circuit schematic*
auxiliary switch assisted neutral generation

Table 1: Third harmonic contributions from various combinations

$-V_{DC}/2$	$-V_{DC}/3$	$-V_{DC}/6$		0			$V_{DC}/6$		$V_{DC}/3$	$V_{DC}/2$
8–7′	8–4′	8–5′	8–3′	8–8′	5–5′	5–3′	5–8′	3–8′	4–8′	7-8'
	8-6'	5–4′	3–4′	3–5′	3–3′	4–4′	4–5′	4–3′	6-8'	
	8–2′	8–1′	5–6′	5–1′	3–1′	4–6′	4-1'	1–8′	2-8'	
	5–7′	5–2′	3–6′	4–2′	1–5′	1–3′	6–5′	6–3′	7–5′	
	3-7'	3–2′	4–7′	6–4′	2–4′	1–1′	2–5′	2–3′	7–3′	
	1–7′	1–4′	1–6′	6-6'	6-2'	2–6′	7–4′	6–1′	7–1′	
		1–2′	6–7′	2–2′	7–7′		2–1′	7–6′	1–1′	
		2–7′					7–2′			

contribute to the triplen harmonics. The space phasor combinations and the voltage space phasor positions used in this strategy are shown (solid lines) in Fig. 5.

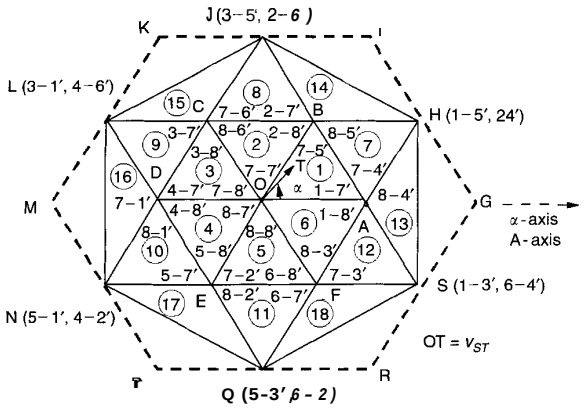

Fig. 5 Space phusor cornhinutions used in proposed PWM strategy

4 Proposed switching strategy and PWM pattern generation

4.1 Sub-hexagons, sectors and timing definitions

The 64 voltage space phasor locations form the vertices of 24 equilateral triangles, referred to as 24 sectors (Fig. 3). Six adjacent sectors together form a hexagon. Six such hexagons can be identified with their centres located at A, B, C, D, E and F, respectively. In addition, there is one inner hexagon with its centre at **O**. As the space phasor combinations at the vertices of the outer hexagon 'GIKMPR (Fig. 3) are not to be used in the proposed PWM strategy, alternative numbering has been assigned to the sectors as shown in Fig. 5. For the remaining part of this paper, the equilateral triangles numbered 1 to 6 are referred to as inner sectors. The equilateral triangles numbered 7 to 12 are referred to as middle sectors. The obtuse-angled isosceles triangles numbered 13 to 18 are referred to as outer sectors (Fig. 5). The reference voltage space phasor for the space vector modulation is denoted as $\mathbf{v}_{sr}$. The angle subtended by $\mathbf{v}_{sr}$ with the positive a axis is denoted as a (Fig. 5). The symbols T_1 and T_2, respectively, denote the time duration for which the active vectors along the trailing edge and the leading edge of a sector (in which the tip of the reference voltage space phasor is situated) are switched to realise the reference voltage space phasor.

4.2 Sector identification and sampling time period

To implement the PWM pattern, the triangular sector in which the tip of the reference space phasor is situated is identified, together with the subhexagon containing it. Sector identification is based on level comparators along ja, jb and jc axes, which are perpendicular to the a, b and c axes, respectively [6]. Symbols v^*_{ja}, v^*_{jb} and v^*_{jc}, denote the projections of $\mathbf{v}_{sr}$ onto the ja, jb and the jc axes, respectively. It may be verified that the tip of $\mathbf{v}_{sr}$, the reference voltage space phasor, is situated in sector 1 if:

$$v^*_{ja} < (\sqrt{3}/4)V_{DC}; v^*_{jb} \geq -(\sqrt{3}/4)V_{DC}; v^*_{jc} < (\sqrt{3}/4)V_{DC} \quad (1)$$

An inspection for the affirmation of the above condition helps to confirm whether the tip of $\mathbf{v}_{sr}$ is situated in sector 1. A similar procedure is adopted for the identification of the other sectors.

The PWM strategy adopted is based on whether the **tip** of the reference voltage space phasor is situated in the inner sectors (1 to 6), or in the middle sectors (7 to 12) or in the outer sectors (13 to 18, Fig. 5). In the following Sections the PWM strategies adopted for the above three cases are explained. Each cycle of the load phase voltage is divided into 48 equal subintervals. Each subinterval duration corresponds to sampling interval T_s. This division is maintained for the entire modulation range with V/f as control. The rated frequency of the induction motor corresponds to the maximum value of the magnitude of the reference voltage space phasor on the boundary of modulation (radius of the circle inscribed in the hexagon HJLNQS, Fig. 5).

4.3 Space phasor based PWM switching strategy for inner sector::

If the tip of the reference voltage space phasor lies in the inner hexagon with centre at **O** (Fig. 5), a space phasor-based scheme as suggested in reference [8] is adopted. In this scheme a space phasor-based PWM strategy is proposed, based on the instantaneous values of reference voltages of the a, b, c phases only. The symbols T_{ga}, T_{gb} and T_{gc}, respectively denote the time duration for which each of the phases for a given inverter is connected to the positive bus of that inverter in a sampling time period T_s and are referred to as inverter leg switchmg timings. This method is extended for the dual inverter scheme (for PWM pattern generation in inner sectors 1 to 6) by clamping an inverter at one end of the load phase while the inverter at the other end is switched. For example, inverter 1 is clamped to a zero state (state 8 or state 7) for a given sampling time period, while inverter 2 is switched in such a way that there is only one switching for each subinterval of that sampling time period (ex: 8′–5′–4′–7′). During the next sampling time period inverter *2* is clamped to a zero state while inverter 1 is switched. This ensures that each inverter is switched for the same duty in one cycle of the load phase voltage. This switching strategy also ensures that each inverter is switched for $n/2$ times with half the DC-link voltage compared to a conventional single inverter scheme switching for n times in one cycle of the load phase voltage. The actual switching time for each inverter leg is obtained in the same way as that of the single inverter scheme [8]. Table 2 gives a detailed description of the switching sequence. It may be noted that, corresponding to the sampling time interval $a = 0$, inverter 1 is clamped to the state 8 while inverter *2* is switched through states 8′–5′–4′–7′. It may also be seen that, corresponding to the sampling time intervals $a = 7.5°$ and $\alpha = 15°$, inverter 2 is clamped to state 7', while inverter 1 is switched through states 8–1–2–7 and 7–2–1–8. When $\alpha = 22.5°$, inverter 1 is clamped to state 8 and inverter 2 is switched through 7′–4′–5′–8′. It may therefore **be** observed that, in a duration of four sampling time intervals, each inverter is switched for two sampling time intervals: ensuring an equal duty for both inverters.

4.4 Mapping middle sectors and outer sectors into the inner hexagon

The outer sectors are isosceles triangles (not equilateral triangles as in the case of the inner sectors 1 to 6) because the inverter switching vector locations G, **I,** K, M, P, R (Fig. 6) are forbidden in the proposed PWM strategy. In Fig. 6, reference voltage vectors $\mathbf{OV_1}$ and $\mathbf{OV_2}$ at two

Table 2 Switching sequences in all the sectors

α (deg.)	possible sectors			switching sequences inner sectors $T_0/2$–T_2–T_1–$T_0/2$	 middle sectors $T_0/2$–T_2–T_1–Td2	 outer sectors T_1–T_0–T_2
0.0	1	—	13	88′–85′–84′–87′	—	13′–18′–15′
7.5	1	7	13	77′–27′–17′–87′	17′–27′–24′–74′	64′–74′–24′
15.0	1	7	13	77′–27′–17′–87′	17′–27′–24′–74′	64′–74′–24′
22.5	1	7	13	88′–85′–84′–87′	84′–85′–15′–18′	13′–18′–15′
30.0	1	7	13	88′–18′–28′–78′	85′–15′–18′–28′	24′–24′–15′
37.5	1	7	14	77′–74′–75′–78′	27′–24′–74′–75′	24′–27′–26′
45.0	1	7	14	77′–74′–75′–78′	27′–24′–74′–75′	24′–27′–26′
52.5	1	7	14	88′–18′–28′–78′	85′–15′–18′–28′	15′45′–35′
60.0	2	—	14	88′–38′–28′–78′	—	15′–85′–35′
67.5	2	8	14	77′–76′–75′–78′	75′–76′–26′–27′	24′–27′–26′
75.0	2	8	14	77′–76′–75′–78′	75′–76′–26′–27′	24′–27′–26′
82.5	2	8	14	88′–38′–28′–78′	28′–38′–35′–85′	15′–85′–35′
90.0	2	8	14	88′–85′–86′–87′	38′–35′–85′–86′	26′–26′–35′
97.5	2	8	15	77′–27′–37′–87′	76′–26′–27′–37′	26′–76′–46′
105.0	2	8	15	77′–27′–37′–87′	76′–26′–27′–37′	26′–76′–46′
112.5	2	8	15	88′–85′–86′–87′	38′–35′45′46′	35′–38′–31′
120.0	3	—	15	88′–81′–86′–87′	—	35′–38′–31′
127.5	3	9	15	77′–47′–37′–87′	37′–47′–46′–76′	26′–76′–46′
135.0	3	9	15	77′–47′–37′–87′	37′–47′–46′–76′	26′–76′–46′
142.5	3	9	15	88′41′–86′–87′	86′41′–31′–38′	35′–38′–31′
150.0	3	9	15	88′–38′–48′–78′	81′–31′–38′–48′	46′–46′–31′
157.5	3	9	16	77′–76′–71′–78′	47′–46′–76′–71′	46′–47′–42′
165.0	3	9	16	77′–76′–71′–78′	47′–46′–76′–71′	46′–47′–42′
172.5	3	9	16	88′–38′–48′–78′	81′–31′–38′–48′	31′–81′–51′
180.0	4	—	16	88′–58′–48′–78′	—	31′41′–51′
187.5	4	10	16	77′–72′–71′–78′	71′–72′–42′–47′	46′–47′–42′
195.0	4	10	16	77′–72′–71′–78′	71′–72′–42′–47′	46′–47′–42′
202.5	4	10	16	88′–58′–48′–78′	48′–58′–51′–81′	31′–81′–51′
210.0	4	10	16	88′41′–82′–87′	58′–51′–81′–82′	42′–42′–51′
217.5	4	10	17	77′–47′–57′–87′	72′–42′–47′–57′	42′–72′–62′
225.0	4	10	17	77′–47′–57′–87′	72′–42′–47′–57′	42′–72′–62′
232.5	4	10	17	88′–81′–82′–87′	58′–51′–81′–82′	51′–58′–53′
240.0	5	—	17	88′–83′–82′–87′	—	51′–58′–53′
247.5	5	11	17	77′–67′–57′–87′	57′–67′–62′–72′	42′–72′–62′
255.0	5	11	17	77′–67′–57′–87′	57′–67′–62′–72′	42′–72′–62′
262.5	5	11	17	88′–83′–82′–87′	82′–83′–53′–58′	51′–58′–53′
270.0	5	11	17	88′–58′–68′–78′	83′–53′–58/48′	62′–62′–53′
277.5	5	11	18	77′–72′–73′–78′	67′–62′–72′–73′	62′–67′–64′
285.0	5	11	18	77′–72′–73′–78′	67′–62′–72′–73′	62′–67′–64′
292.5	5	11	18	88′–58′48′–78′	83′–53′–58′–68′	53′–83′–13′
300.0	6	—	18	88′–18′68′–78′	—	53′43′–13′
307.5	6	12	18	77′–74′–73′–78′	73′–74′–64′–67′	62′–67′–64′
315.0	6	12	18	77′–74′–73′–78′	73′–74′–64′–67′	62′–67′–64′
322.5	6	12	18	88′–18′–68′–78′	68′–18′–13′–83′	53′–83′–13′
330.0	6	12	18	88′–83′–84′–87′	18′–13′–83′–84′	64′44′–13′
337.5	6	12	13	77′–67′–17′–87′	74′–64′–67′–17′	64′–74′–24′
345.0	6	12	13	77′–67′–17′–87′	74′–64′–67′–17′	64′–74′–24′
352.5	6	12	13	88′–83′–84′–87′	18′–13′–83′–84′	13′–18′–15′

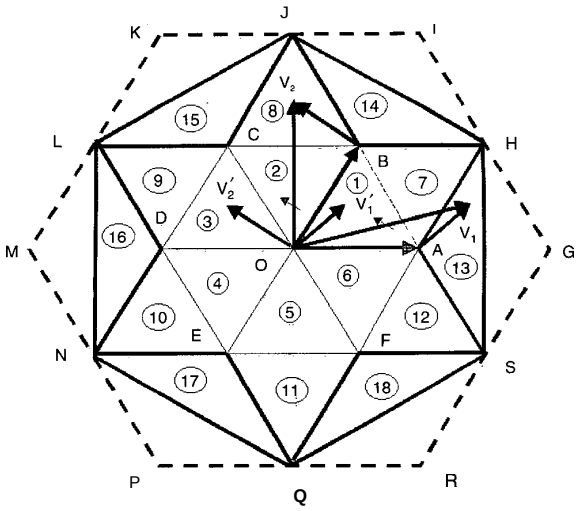

Fig. 6 *Resolution of reference voltage space phasor in middle rind outer sectors*

different time instants are shown with their tips lying in sectors 13 and 8, respectively. In sector 13 vector $\mathbf{OV_1}$ can be generated using vectors $\mathbf{OA}$ and $\mathbf{AV_1}$. Vector $\mathbf{OA}$ can readily be obtained from the appropriate space phasor combinations from the individual inverters (Fig. 5). Vector $\mathbf{AV_1}$ is not directly available from the space phasor combinations (Fig. 5) and hence is generated from adjacent active switching vector locations using volt–sec balance. In sector 13 vector $\mathbf{AV_1}$ can be realised by switching between vectors **OA, OH** and **OS** for periods T_0, T_1 and T_2, respectively, in a sampling period T_s. Periods T_0, T_1 and T_2 for vector $\mathbf{AV_1}$ in sector 13 can be found out by mapping vector $\mathbf{AV_1}$ to $\mathbf{OV'_1}$ by shifting point A to **O.** By shifting point A to **O,** the outer isosceles triangle ASH is mapped to an inner isosceles triangle OFB (Fig. 6). Similarly, sector 8 can be mapped to inner sector 3 by shifting point B to **O.** In this case, vector $\mathbf{BV_2}$ gets mapped to $\mathbf{OV'_2}$. Adopting this procedure, all middle sectors (7 to 12) can be mapped into the corresponding inner sectors, and all outer sectors (13 to 18) can be mapped into the corresponding inner isosceles triangles.

4.5 Space phasor based PWM switching strategy for middle sectors

By shifting the centres of subhexagons A to F to point **O** using an appropriate coordinate transformation, middle sectors 7 to 12 get mapped to a corresponding inner sector (1 to 6). Once the mapped inner sector is identified, switching periods for individual legs (T_{ga}, T_{gb} and T_{gc}) for both the inverters may be obtained using the procedure outlined in reference [8]. There exists an explicit relationship between the inverter leg switching timings (T_{ga}, T_{gb} and T_{gc}) and the space vector switching timings (T_0, T_1 and T_2), depending upon the sector of the inner hexagon in which the tip of the transformed reference space vector $\mathbf{OV'_2}$ is situated. Using these relationships, the space vector switching timings T_0, T_1 and T_2 can be determined from the inverter leg switching timings T_{ga}, T_{gb} and T_{gc}. For example, if the tip of $\mathbf{OV_2}$ is situated in sector 7, subhexagonal centre A is shifted to **O** if $0" < a < 30"$ mapping sector 7 to sector 2 in the inner hexagon. If $30° \leq a < 60°$, to ensure that the nearest subhexagonal centre is shifted to **O,** the subhexagonal centre B is shifted to O mapping sector 7 to sector 6 in the inner hexagon.

It may easily be verified that:

$$T_0 = 2T_{gc};\ T_1 = T_{ga} - T_{gc};\ T_2 = T_{gb} - T_{ga} \quad \text{when sector 7 is mapped to sector 2} \tag{2a}$$

and

$$T_0 = 2T_{gb};\ T_1 = T_{gc} - T_{gb};\ T_2 = T_{ga} - T_{gc} \quad \text{when sector 7 is mapped to sector 6} \tag{2b}$$

A similar procedure is adopted when the tip of $\mathbf{OV_2}$ is situated in sectors 8 to 12. Table 3 summarises the relationship amongst T_1, T_2 and T_0 and $T_{,,,}$ T_{gb} and $T_{,,}$ for all of the middle sectors. The appropriate active vectors for the middle sectors are switched as depicted in Table 2.

Table 3: Relationship between T_0, T_1 and T_2 and T_{ga}, T_{gb} and T_{gc} in the middle sectors

range of 'a	sector before trans-forma-tion	sector after trans-forma-tion	$T_{0/2}$	T_1	T_2
$0" \leq a < 30"$	7	2	T_{gc}	$T_{ga}-T_{gc}$	$T_{gb}-T_{ga}$
$30" \leq \alpha < 60"$	7	6	T_{gb}	$T_{gc}-T_{gb}$	$T_{ga}-T_{gc}$
$60" \leq \alpha < 90"$	8	3	T_{ga}	$T_{gb}-T_{gc}$	$T_{gc}-T_{ga}$
$90" \leq a < 120"$	8	1	T_{gc}	$T_{ga}-T_{gb}$	$T_{gb}-T_{gc}$
$120" \leq a < 150"$	9	4	T_{ga}	$T_{gb}-T_{ga}$	$T_{gc}-T_{gb}$
$150" \leq a < 180"$	9	2	T_{gc}	$T_{ga}-T_{gc}$	$T_{gb}-T_{ga}$
$180" \leq a < 210"$	10	5	T_{gb}	$T_{gc}-T_{ga}$	$T_{ga}-T_{gb}$
$210" \leq \alpha < 240"$	10	3	T_{ga}	$T_{gb}-T_{gc}$	$T_{gc}-T_{ga}$
$240" \leq \alpha < 270"$	11	6	T_{gb}	$T_{gc}-T_{gb}$	$T_{ga}-T_{gc}$
$270" \leq a < 300"$	11	4	T_{ga}	$T_{gb}-T_{ga}$	$T_{gc}-T_{gb}$
$300" \leq a < 330"$	12	1	T_{gc}	$T_{ga}-T_{gb}$	$T_{gb}-T_{gc}$
$330" \leq \alpha < 360"$	12	5	T_{gb}	$T_{gc}-T_{ga}$	$T_{ga}-T_{gb}$

4.6 Space phasor based PWM switching strategy for outer sectors

The procedure outlined for the middle sectors may be extended further to the outer sectors. The outer sectors are obtuse-angled isosceles triangles (Fig. 6) and may be mapped into the inner hexagon by shifting the centres of the respective subhexagon centres to point **O.** For example, if the tip of the reference voltage space phasor is situated in sector 13 (Fig. 6), a co-ordinate transformation to shift the subhexagonal centre **A** to O maps sector 13 **(ASH)** into sector OFB. As a consequence, vector $\mathbf{AV_1}$ is mapped to vector $\mathbf{OV'_1}$. Switching periods T_0, T_1 and T_2 for realising vector $\mathbf{OV'_1}$ in sector OFB may be determined using the volt–sec balance. In the analysis presented in Appendix 8, $|\mathbf{OV'_1}|$ is denoted by $|v'_{sr}|$ and $\angle AOV'_1 = \phi$. It may be seen that $|\mathbf{OB}| = |\mathbf{OF}| = V_{DC}/2$ (Fig. 6). The symbols v_a^*, v_b^* and v_c^* denote the instantaneous values of the actual reference phase voltages and are obtained by projecting the tip of the actual reference voltage space phasor $\mathbf{OV_1}$ onto the respective phase axes and multiplying by a factor of (2/3). Similarly, symbols v_a, v_b and v_c denote the instantaneous values of the modified reference phase voltages and are obtained by projecting the tip of the mapped reference voltage space phasor $\mathbf{OV'_1}$ onto the respective phase axes

and multiplying by a factor of (2/3). The factor of (2/3) arises out of the conventional α-β to abc transformation,

$$\begin{bmatrix} v_a \\ v_b \\ v_c \end{bmatrix} = \begin{bmatrix} 2/3 & 0 \\ -1/3 & 1/\sqrt{3} \\ -1/3 & -1/\sqrt{3} \end{bmatrix} \begin{bmatrix} v_\alpha \\ v_\beta \end{bmatrix} \quad (3)$$

Table4 depicts the relationship between T_1, T_2 and T_0 in the outer sectors and the instantaneous values of the transformed reference phase voltages v_a, v_b and v_c. It may be noted from these expressions that the timing duration T_1 and T_2 can be obtained directly from the instantaneous reference phase values as in the case of the inner sectors.

Table 4 Relationship between active vector switching times T_1 and T_2 and the instantaneous values of the transformed reference phase voltages

sector before transformation	sector after transformation	T_1	T_2
ASH	OFB	$(2T_s/V_{DC})\ (v_a - v_b)$	$(2T_s/V_{DC})\ (v_a - v_c)$
BHJ	OAC	$(2T_s/V_{DC})\ (v_a - v_c)$	$(2T_s/V_{DC})\ (v_b - v_c)$
CJL	OBD	$(2T_s/V_{DC})\ (v_b - v_c)$	$(2T_s/V_{DC})\ (v_b - v_a)$
DLN	OCE	$(2T_s/V_{DC})\ (v_b - v_a)$	$(2T_s/V_{DC})\ (v_c - v_a)$
ENQ	ODF	$(2T_s/V_{DC})\ (v_c - v_a)$	$(2T_s/V_{DC})\ (v_c - v_b)$
FQS	OEA	$(2T_s/V_{DC})\ (v_c - v_b)$	$(2T_s/V_{DC})\ (v_a - v_b)$

Thus in all (inner, middle and outer) sectors, the respective inverter vector switching periods can easily be obtained from the instantaneous values of the sampled reference phase voltages.

4.7 Over-modulation

When the reference vector is located outside the hexagon HJLNQS (Fig. 5), a modified reference voltage vector on the periphery of the hexagon is chosen with the same angle as the original reference vector [4]. The modified active vector switching times T_1' and T_2' during overmodulation with the modified reference voltage vector may be calculated simply by the following conditions:

$$T_1' + T_2' = T_s \quad \text{and} \quad T_1' : T_2' :: T_1 : T_2 \quad (4)$$

Therefore,

$$T_1' = \{T_1/(T_1 + T_2)\}.T_s;\ T_2' = \{T_2/(T_1 + T_2)\}.T_s \quad (5)$$

5 Experimental results and discussion.

The proposed scheme is implemented for a 1 HP, 3-phase, open-end induction motor drive in open loop with *V/f* control for different reference voltages covering the entire speed range.

Experimental results for $|v_{sr}| = 0.4 v_{DC}$ are presented in Figs. 7 and 8. In this case, the tip of the reference voltage space phasor v_{sr} is confined to the inner sectors (i.e. sectors 1 to 6, Fig. 5).

Fig. 7 shows the actual motor phase voltage waveform obtained experimentally. The motor phase current waveform obtained experimentally is shown in Fig. 8. It is a familiar waveform in the literature and it is known that this waveform does not contain the harmonics of the triplen order. Elimination of the triplen harmonic components in

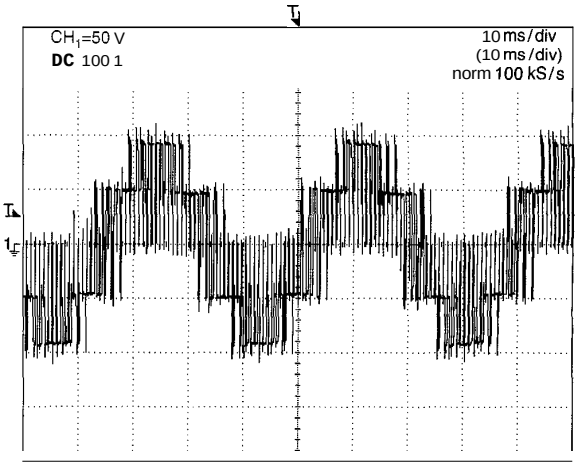

Fig. 7 *Actual motor phase voltage without tripen harmonic components for* $|v_{sr}| = 0.4 V_{DC}$
scale: y-axis: 50 V/div; x-axis: 10 ms/div

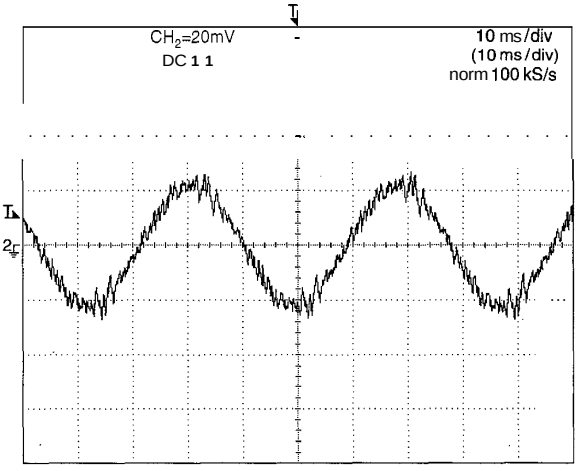

Fig. 8 *Motor phase current at no-load for* $|v_{sr}| = 0.4 V_{DC}$
scale: y-axis: 1 amp/div; x-axis: 10 ms/div

the actual motor phase voltage is achieved by generation of the switched neutral as explained in Section 3.

Similar experimental results are presented for the case when $|v_{sr}|$ is equal to 0.6 V_{DC} (Figs. 9–12). In this case, the tip of the reference voltage space phasor is situated either in the middle sectors (7 to 12) or in the outer sectors (13 to 18, Fig. 5). Fig. 9 shows the pole voltages (v_{ao} and $v_{a'o}$) of the individual inverters (top and bottom traces), while the middle trace shows $v_{aa'}$, the difference of these two pole voltages. All the traces of Fig. 9 have been obtained from the gate drive signals of the two inverters. Figs. 10 and 11, respectively, show the actual inverter voltage waveform and the motor phase current at no-load. The harmonic spectrum of the actual motor phase voltage (shown in Fig. 10) is shown in Fig. 12. The absence of the triplen harmonics in the harmonic spectrum of the motor phase voltage (Fig. 12) shows the capability of the proposed power circuit topology and the PWM strategy to eliminate the triplen harmonic components. Figs. 13–16 show the experimental results

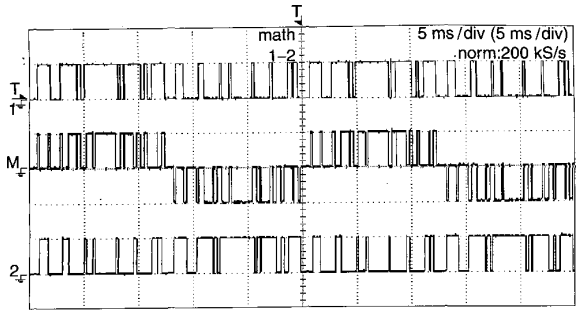

Fig. 9 *Individual pole voltages v_{ao} and $v_{d'o}$ for $|v_{sr}| = 0.6V_{DC}$ (top and bottom traces) voltage v_{ad} $(v_{ao}-v_{d'o})$ containing triplen harmonic components (middle trace)*

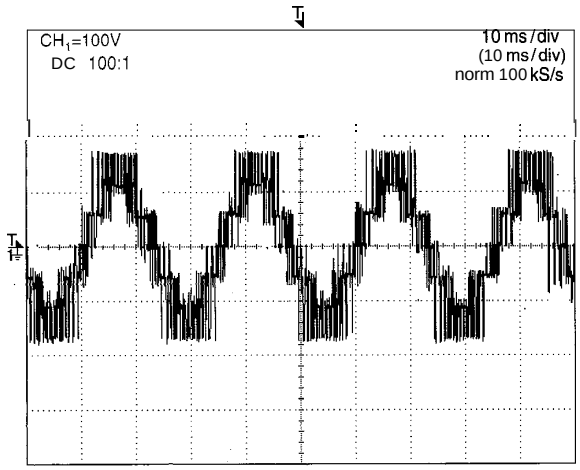

Fig. 10 *Actual motor phase voltage without triplen harmonic components for $|v_{sr}| = 0.6V_{DC}$*
scale: y-axis: 100V/div; x-axis: 10ms/div

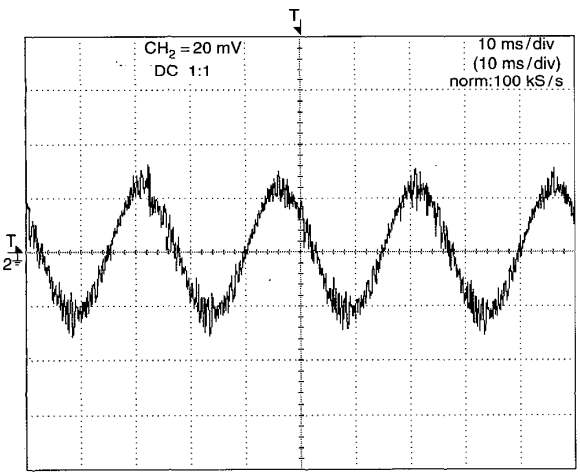

Fig. 11 *Motor phase current at no-load for $|v_{sr}| = 0.6V_{DC}$*
scale: y-axis: 1amp/div; x-axis: 10ms/div

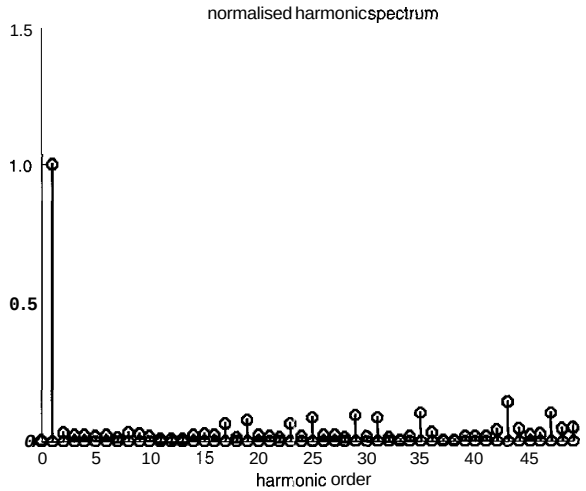

Fig. 12 *Normalised harmonic spectrum of motor phase voltage for $|v_{sr}| = 0.6V_{DC}$*

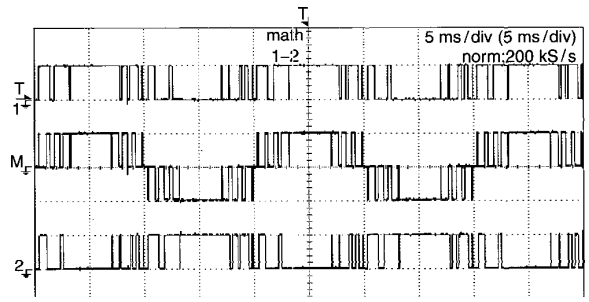

Fig. 13 *Individual pole voltages v_{ao} and $v_{d'o}$ for $|v_{sr}| = 0.9V_{DC}$ (top and bottom traces) voltage v_{ad} $(v_{ao}-v_{d'o})$ (middle trace)*

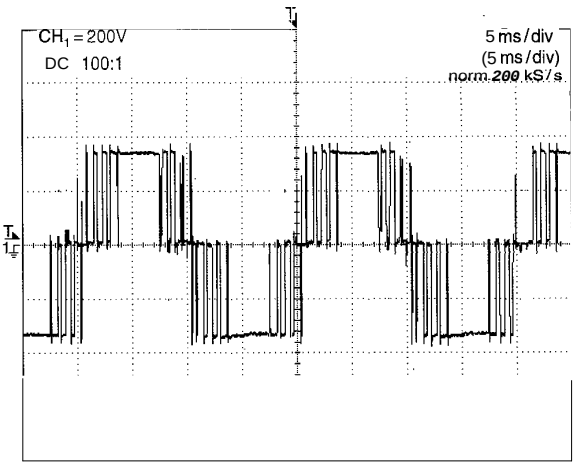

Fig. 14 *Actual motor phase voltage for $|v_{sr}| = 0.9V_{DC}$*
scale: y-axis: 200V/div; x-axis: 5ms/div

when $|V_{sr}| = 0.9V_{DC}$ and corresponds to the case of overmodulation as $|V_{sr}| > 0.75\ V_{DC}$ (Fig. 5). In this case the tip of the reference voltage space phasor is forced to trace the hexagon HJLNQS (Fig. 5) as explained in Section 4.7, During overmodulation, space vector combinations at locations H, J, L, N. Q and S are used exclusively (Fig. 5) as the subinterval T_0, in the sampling time period T_s, is zero in this case. Triplen harmonics are absent in this case as space phasor combinations at H (1–5′, 2–4′), J (3–5′, 2–6′), L (3–1′, 4–6′), N (5–1′, 4–2′), Q (5–3′, 6–2′) and S (1–3′, 6–4′)

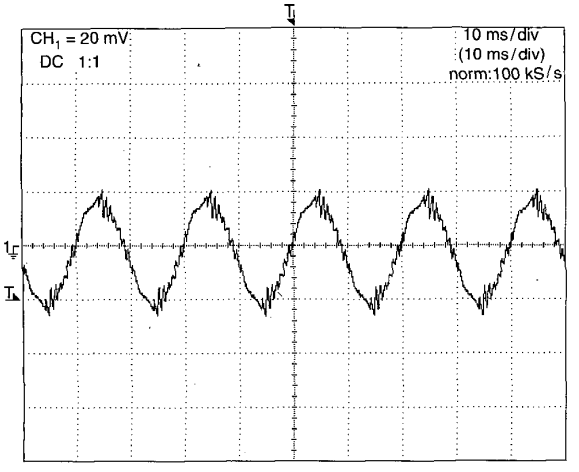

Fig. 15 *Motor phase current at no-loadfor* $|v_{sr}| = 0.9V_{DC}$
scale: y-axis: 1 amp/div; x-axis: 10ms/div

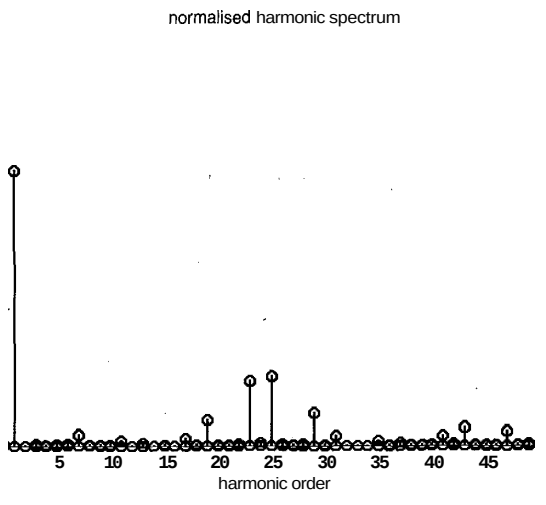

Fig. 16 *Normalised harmonic spectrum of* v_{ad} *and motor phase voltage for* $|v_{sr}| = 0.9V_{DC}$
triplen harmonic content in v_{ad} is zero in this case

(Fig. 5), used for the PWM generation, will not contribute to triplen harmonic components (Table 1). Consequently, it is expected that V_{ad} does not possess any triplen harmonic content in this case.

The top and bottom traces of Fig. 13 show the pole voltages of individual inverters v_{ao} and $v_{d'o}$, respectively, while the middle trace shows v_{ad}, the difference of these pole voltages. Figs. 14 and 15, respectively, show actual motor phase voltage and motor phase current. It may be observed that the waveform of v_{ad} (middle trace, Fig. 13) is identical to the motor phase voltage (Fig. 14). Thus, it is evident that experimental results are in agreement with theoretical assertion that the triplen harmonic content in v_{ad} in this case is zero.

Thus, for the dual-inverter fed open-end winding induction motor, triplen harmonic elimination has been achieved using proposed power circuit topology and the associated PWM scheme (auxiliary switch assisted neutral generation). The power circuit topology obviates isolation transformers or harmonic filters that are bulky and expensive.

6 Conclusion

(i) **A** dual two-level inverter fed open-end winding induction motor drive has been proposed. The proposed scheme produces voltage space phasor locations similar to that of a three-level inverter.

(ii) A PWM switching strategy aimed to suppress the triplen harmonic currents is also proposed, eliminating the need for bulky harmonic filters or isolation transformers.

(iii) The elimination of triplen harmonic currents is achieved by generation of a switched neutral using bidirectional auxiliary switches.

(iv) In the proposed power circuit, each inverter switching frequency is half that of the motor phase switching frequency.

(v) The DC link capacitors carry only ripple current and not load current. Hence split-level voltage fluctuations are avoided in the proposed scheme, when compared to a conventional three-level inverter.

(vi) A simple space phasor-based PWM scheme is proposed, which requires only the instantaneous sampled values of the reference phase voltages for gate drive signal generation over the entire speed range.

(vii) The switching patterns are so devised that in each inverter only one leg is switched during a subinterval of the sampling period T_s.

(viii) However, this scheme requires four bidirectional switches (each switch consisting of four diodes and one IGBT) and thus four additional gate drive circuits.

7 References

1 NABAE, A., TAKAHASHI, I., and AGAKI, H.: 'A new neutral-point-clamped PWM inverter', *IEEE Trans.*, 1981, **IA–17,** pp. 518–523
2 BHAGWAT, P.M., and STEFANOVIC, V.R.: 'Generalized structure of a multi level PWM inverter', *JEEE Truns.*, 1983, **IA-19, pp.** 1057–1069
3 MWINYIWIWA, B., and WOLANSKT, 2.: 'Multimodular multilevel converters with input/output linearity', *JEEE Trans.*, 1997, **33,** (5), pp. 1214–1219
4 RUFER, A., VEENSTRA, M., and GOPAKUMAR, K.: 'Asymmetric multilevel converter for high resolution voltage phasor generation'. *EPE'99*, Lausanne, **pp.** PI–PI0
5 STEMMLER, H., and GUGGENBACH, P.: 'Configurationsof high power voltage source inverter drives'. *EPE conference*, 1993, pp. 7–i2
6 SHIVAKUMAR, E.G., GOPAKUMAR, K., and RANGANATHAN, V.T.: 'Space vector PWM control of dual inverter fed open-end winding induction motor drive'. *IEEE-APEC-2000*, **pp.** 394–404
7 Space phasor based pulse width modulated dual inverter switching strategy for an open-end winding induction motor drive for triplen harmonic suppression Indian patent 133/MAS/200/2001
8 KIM, J.-S., and SUL, S.-K.: 'A novel voltage modulation technique of the space vector PWM'. *JPEC-1995*, pp. 742–747

8 Appendix

8.1

From Fig. 6, the eqn. for the volt–sec balance is given by:

$$|v'_{sr}|\angle\phi.T_s = (V_{DC}/2)\angle -60^0.T_1 + (V_{DC}/2)\angle 60^0.T_2 \quad (6)$$

$$\text{where } |v'_{sr}|\cos\phi = v_\alpha \quad \text{and} \quad |v'_{sr}|\sin\phi = v_\beta \quad (7)$$

$$\text{with the constraint } T_1 + T_2 + T_0 = T_s \quad (8)$$

From the conventional α-β to *abc* transformation, following (3),

$$v_\alpha = (3/2)v_a \quad \text{and} \quad v_\beta = (\sqrt{3}/2)(v_b - v_c) \quad (9)$$

There is an additional constraint arising out of the three-phase system:

$$v_a + v_b + v_c = 0 \quad (10)$$

From (6) to (10), it may be shown that:

$$T_1 = 2T_s(v_a - v_b)/V_{DC} \quad (11)$$

and

$$T_2 = 2T_s(v_a - v_c)/V_{DC} \quad (12)$$

In a similar way, expressions for T_1 and T_2 in the other outer sectors (14 to 18) may be determined by mapping these sectors into the corresponding inner sectors for any set of instantaneous reference phase values v_a*, v_b* and v_c*. Timing duration T_0 is determmed from (8). Expressions for T_1 and T_2 in all the sectors have been presented in Table 4.

8.2

Motor parameters (1HP, three-phase, four-pole-induction motor)

$R_s = 2.08$ ohms, $R_r = 1.19$ ohms, $X_s = 2.26$ ohms, $X_r = 2.26$ ohms, $M = 2.15$ ohms